INTERNATIONAL JOURNAL OF CLIMATOLOGY
Int. J. Climatol. **33**: 210–227 (2013)
Published online 17 January 2012 in Wiley Online Library
(wileyonlinelibrary.com) DOI: 10.1002/joc.3415

RMetS
Royal Meteorological Society

How much can air conditioning increase air temperatures for a city like Paris, France?

Cécile de Munck,[a]* Grégoire Pigeon,[a] Valéry Masson,[a] Francis Meunier,[b] Pierre Bousquet,[b] Brice Tréméac,[b] Michèle Merchat,[c] Pierre Poeuf[c] and Colette Marchadier[a]

[a] *CNRM/GAME, Météo France, 42 avenue Gaspard Coriolis, 31 057 Toulouse Cedex, France*
[b] *LGP2ES (EA21), CNAM IFFI, Case 331, 292 rue Saint Martin, 75 141 Paris Cedex 03, France*
[c] *Climespace, 185 rue de Bercy, 75 012 Paris, France*

ABSTRACT: A consequence of urban heat islands in summer is an increase in the use of air conditioning in urbanized areas, which while cooling the insides of buildings, releases waste heat to the atmosphere. A coupled model consisting of a meso-scale meteorological model (MESO-NH) and an urban energy balance model (TEB) has been used to simulate and quantify the potential impacts on street temperature of four air conditioning scenarios at the scale of Paris. The first case consists of simulating the current types of systems in the city and was based on inventories of dry and evaporative cooling towers and free cooling systems with the river Seine. The other three scenarios were chosen to test the impacts of likely trends in air conditioning equipment in the city: one for which all evaporative and free cooling systems were replaced by dry systems, and the other two designed on a future doubling of the overall air conditioning power but with different technologies. The comparison between the scenarios with heat releases in the street and the baseline case without air conditioning showed a systematic increase in the street air temperature, and this increase was greater at nighttime than day time. It is counter-intuitive because the heat releases are higher during the day. This is due to the shallower atmospheric boundary layer during the night. The increase in temperature was 0.5 °C in the situation with current heat releases, 1 °C with current releases converted to only sensible heat, and 2 °C for the future doubling of air conditioning waste heat released to air. These results demonstrated to what extent the use of air conditioning could enhance street air temperatures at the scale of a city like Paris, and the importance of a spatialized approach for a reasoned planning for future deployment of air conditioning in the city. Copyright © 2012 Royal Meteorological Society

KEY WORDS meso-scale atmospheric modelling; air conditioning; urban micro-climate; urban heat island

Received 15 June 2011; Revised 21 October 2011; Accepted 23 November 2011

1. Introduction

During the 2003 European heat wave, which could be representative of a normal summer by the end of the century (Déqué, personal communication), the urban heat island (UHI) observed in Paris, with temperatures up to 8 °C higher in central Paris than in the countryside, exacerbated the heat stress situation. Paris is faced with an increasing urban population, a specific micro-climate, and recent episodes of high summer temperatures. In this context, the cooling requirements for the city of Paris, in order to cool or maintain constant the temperature of goods and people for health, comfort, commercial and industrial reasons, could increase. Current energy demand projections suggest that air conditioning (AC) usage is likely to increase significantly in the short term. The Energy Efficiency and Certification of Central Air Conditioners Report commissioned in 2003 by the European Union (Adnot, 2003b) forecasts a doubling of the energy consumption due to AC by 2020 in France. Hence, considering that the use of AC systems, while cooling the insides of buildings, releases waste heat to the lower part of the urban atmosphere, it is legitimate to question its effect on the local climate at the scale of the city. What is the order of magnitude of potential impacts on street air temperatures? Are they localized or spread out? Do they worsen during the day or during the night? Are they dependent on the density of AC installations and the cooling technology implemented such as dry and evaporative cooling towers and free cooling systems?

Literature is scarce on the effects of AC on urban microclimates worldwide. Surprisingly, the literature on North American urban areas (Akbari *et al*., 2001; Akbari and Konopacki, 2004; Salamanca *et al*., 2011) or European cities, such as Athens (Hassid *et al*., 2000) and London (Kolokotroni *et al*., 2006), mainly focuses on the impact of the urban heat islands on AC-related energy consumption/demand but not on the feedback on outdoor temperatures. On this point, studies were only found for one North American city (Houston) and three Asian cities (Tokyo, Taipei and Wuhan), and they differ in the level of sophistication of the models that the authors used and the spatial scale that they focused on. Of those

* Correspondence to: C. de Munck, CNRM/GAME, Météo France, 42 avenue Gaspard Coriolis, 31 057 Toulouse Cedex, France.
E-mail: cecile.demunck@meteo.fr

studies, that of Salamanca *et al*. (2011) investigated the feedbacks of AC systems on outdoor air temperatures at the scale of Houston City (Texas) based on the coupling between a meso-scale model, a multilayer urban canopy model and a simple building energy model. They found an increase in night temperatures of up to 2 °C in the densest areas of Houston. For Tokyo, Ohashi *et al*. (2007) have simulated a 1–2 °C increase in air temperatures in the office districts due to AC usage during week days, by using a multilayer urban canopy model and a building energy analysis model. Kikegawa *et al*. (2003) used a coupled model consisting of a building energy analysis model, an urban canopy model and a meso-scale meteorological model. Their simulation results were focussed on a single office district in central Tokyo and corroborate Ohashi *et al*. (2007) findings, with an average 1 °C increase in street air temperature across three air conditioner-placement scenarios. The Hsieh *et al*. (2007) study, based on a building energy software (EnergyPlus) and a computational fluid dynamics software (Windperfect), shows a similar effect on street air temperature for the densest residential district of Taipei city where buildings were equipped with window-type air conditioners: a local temperature rise between 0.78 °C and 1.84 °C, with the maximum rise occurring between 23 : 00 and 24 : 00 h. Contrary to previous studies, figures for the city of Wuhan (China) were obtained by Wen and Lian (2009) based on simple calculations (box model type). They show that domestic air conditioner usage may increase Wuhan City's mean temperature of 0.2 or 2.56 °C, depending on the temperature profile modelled for the city (under normal or inversion conditions, respectively).

However, no estimate of the impacts of different types of cooling technologies on outdoor temperatures has yet been carried out at a larger scale than the neighbourhood with detailed meso-scale models. The present paper describes the methodology implemented to do so at the scale of Paris City. Simulation results are presented for a set of AC scenarios chosen to represent likely equipments for the city, currently (based on the inventory of current AC waste heat emissions) and in the near future.

2. Methodology

2.1. Overview

The methodology implemented in this work (Figure 1) is a numerical atmospheric meso-scale simulation of the 2003 European heat wave for the City of Paris for different scenarios of AC usage. With the aim of comparing and estimating the influence of cooling systems on the street air temperatures and the magnitude of the UHI of Paris City, several configurations/scenarios of AC were simulated (Table I) by varying the form of heat waste discharged to the atmosphere (as sensible or latent heat), the distribution pattern of AC (individual *versus* networked systems) or the intensity of cooling power. The different cases of AC usage are as follows:

(1) without AC to allow referring to a baseline (NO-AC),
(2) with the current types of AC systems coexisting in the city, dry and evaporative cooling towers and free cooling systems (REAL-AC),
(3) with all current AC systems converted to dry cooling systems (DRY-AC),
(4) a future projection of AC, with doubling of the dry waste heat releases (DRY-ACx2),

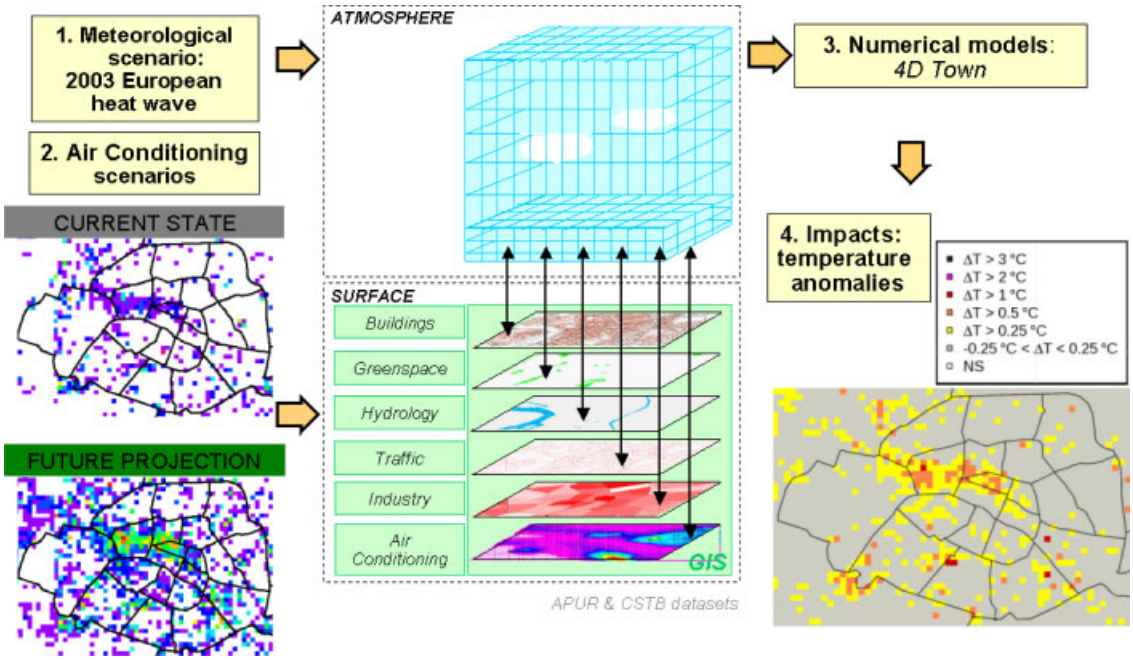

Figure 1. General methodology. This figure is available in colour online at wileyonlinelibrary.com/journal/joc

Table I. Air conditioning scenarios.

Case	Description
NO-AC	A scenario without AC (baseline)
REAL-AC	The current situation with an overall heat release power of 5.16 GW, which encompasses three types of AC systems in the city: • dry air conditioners discharging sensible waste heat to air implemented for individual flats or houses (such as window units) or at the scale of a building (such as rooftop units), • evaporative air conditioners (such as evaporative cooling towers) discharging 95% of latent waste heat and 5% of sensible waste heat to air implemented at the scale of a building or a neighbourhood, with a distribution network, • free cooling systems discharging waste heat to the river Seine and implemented at the scale of a neighbourhood with a district network (such as the ones developed and maintained by the Climespace Company).
DRY-AC	Same overall heat release power than in the REAL-AC case, with conversion of latent heat releases to sensible releases (which implies that all evaporative air conditioners are replaced by dry air conditioners). Moreover, we assume that systems are autonomous and that network districts disappear. Consequently, the heat releases are located where the cooling power is used.
DRY-ACx2	A future projection of AC usage assuming a doubling of the overall power of the heat released over the simulation domain covered only by dry air conditioners. This increase would be mainly due to an increase in usage in the office district. The overall power of the sensible heat released (10.32 GW) is distributed with two thirds in central Paris and one third outside. The distribution is carried out by increasing the power of the grid cells up to what the floor area can allow.
NOAIR-ACx2	A future projection of AC usage for which all the cooling needs for Paris are satisfied by free cooling district networks that do not release their waste heat to air. The cooling power inside the buildings is kept identical to that of scenario DRY-ACx2.

(5) a future projection of AC with the same cooling power as in scenario DRY-ACx2 but without discharging waste heat to air, implying the use of alternative methods for heat discharge (NOAIR-ACx2).

The choice for dry scenarios is based on the assumption that existing evaporative cooling towers (with a lifetime of around 15 years) might be replaced in the future by dry cooling towers because of their heavy maintenance and the fear associated with the risk of legionellosis. Then the nationwide projections of AC usage from Adnot (2003a, 2003b) allowed to choose a realistic figure for future projections of heat releases. Not only is doubling the power of AC releases a realistic hypothesis for the 2020s (even if it is probably underestimated), but its tangible aspect also facilitates the interpretation of simulation outputs.

Finally, the outputs of numerical models were statistically processed to derive two indicators: the temperature anomalies in the streets and the characteristics of Paris heat island.

2.2. Meteorological conditions

We have chosen to simulate the meteorological conditions of the 2003 European heat wave because this heat wave is estimated to be representative in mean temperature of summers of the second half of the 21st century, according to the Météo France global climate model projection (Déqué, personal communication). The characteristics of this heat wave allow us to understand what kind of weather conditions Paris and its inhabitants are likely to face in the future.

The summer of 2003 has been the warmest in France since the establishment of the French weather station network (in 1951). The heat wave observed during the month of August 2003 was notable not only by the amplitude of its maximum temperature but also by its records for night temperatures (above 25 °C on the 11th and 12th of August in the Park Montsouris on the southern outskirts of inner Paris (Figure 2), and its duration (about 2 weeks). There was a gradual rise in temperatures between the 1st and 5th of August (with first record-breaking temperatures in the southwest of France on the 3rd and 4th of August) followed by a period of high heat until the 13th of August, the date of the beginning of the gradual decline in temperatures (Bessemoulin *et al*., 2004). Consequently, we focused on a 6-day simulation period, extending from the 8th to the 13th of August, chosen to be the hottest period of the heat wave. At the scale of France, this period was marked by settled anticyclonic conditions, with dry and stable air masses in the lower layers of the atmosphere which got warmer and warmer until the 14th of August, the date marking the end of the heat wave.

Moreover, Bessemoulin *et al*. (2004) noted that the temperature records of the 11th and 12th of August in Paris were aggravated by the presence of a low wind, which had implications not only in terms of pollution (non-dispersion of pollutants accentuated) but also in terms of health (higher risk of non-cooling of the body). Moisture, which is also recognized as an

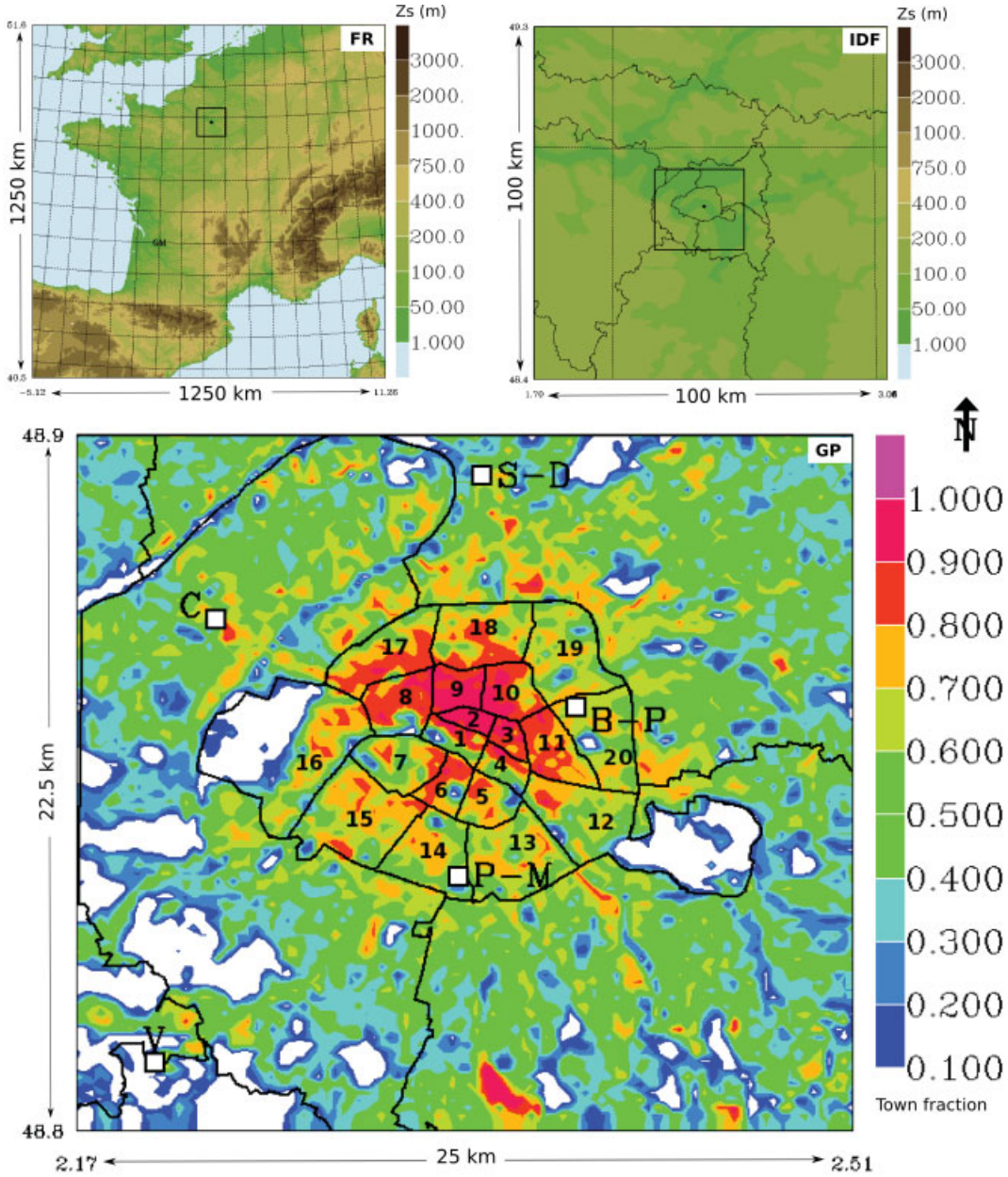

Figure 2. The three-nested simulation domains for the three spatial resolutions (FR: 2.5 km; IDF: 1.25 km; GP: 250 m). Orography (Zs) is shown for FR and IDF, town fraction for GP. On GP domain are also annotated the locations of 5 weather stations (V for Villacoublay, C for Courbevoie, S-D for Saint-Denis, B-P for Belleville-Park, P-M for Paris-Montsouris) and inner Paris district numbers.

aggravating factor in heat waves, has not played a determinant role because the situation remained relatively dry all along that period except for some sporadic storm events. These storms, often occurring in mountainous regions, were also observed over plains, with variable daily precipitation totals (3–35 mm). These precipitation events might have affected the IDF region on the 10th, 11th and 13th of August (Figure A1). Also, the effects of the heat wave over the capital were compounded at nighttime due to the smaller decline in temperatures in the city than in its surroundings (UHI). On the basis of a spatial extrapolation of station records (available at http://climascope.meteo.fr/), it was possible to estimate the intensity of the Paris nighttime heat island during the 2003 heat wave: it reached about 8 °C between the countryside northwest of Paris and central Paris (i.e. for a distance of 65 km), with the mean minimum temperature rising up to 24 °C in central Paris when the countryside peaked at 16 °C. At a smaller scale, between the city centre and the limit of the dense agglomeration of Paris (4 km from Notre Dame Cathedral, Paris), the magnitude of the nighttime heat island was about 4 °C.

2.3. Atmospheric model implementation

The simulations were performed with a coupled model consisting of the non-hydrostatic meso-scale atmospheric model MESO-NH (Lafore *et al.*, 1998; Stein *et al.*, 2000) and four surface-atmosphere energy-exchange models gathered in the SURFEX numerical tool. The implementation of the models actually rely on a combination of

3 nested domains (Stein *et al.*, 2000) of different spatial and temporal resolutions to go down to a 250 m horizontal resolution: the first domain includes all of France (FR, with a size of 500 × 500 grid cells and a 2.5 km resolution, top left of Figure 2), while the second extends to the Île-de-France region (IDF, with a size of 80 × 80 grid cells and a 1.25 km resolution, top right of Figure 2), and the third and last domain focuses on Greater Paris (GP, domain of interest, with a size of 100 × 90 grid cells and a 250 m resolution, bottom of Figure 2). To model the period of interest (8–13 August 2003), the atmospheric model running on FR is initiated and then coupled at its lateral boundaries every 6 h with the analysis of the weather forecasts from the European Centre for Medium-Range Weather Forecasts (ECMWF). Then, the models running on the IDF and GP are nested 2 ways. For the three simulation domains, a vertical grid of 55 levels is used, with a stretched resolution ranging from 30 m at the lowest level to 1000 m at the highest (17 600 m). The simulations are conducted using an Eddy-Diffusivity Mass Flux (EDMF) approach. The mass flux scheme (Pergaud *et al.*, 2009) simulates boundary layer thermals (and cumuli clouds if any). The turbulence scheme (Cuxart *et al.*, 2000) uses a Turbulent Kinetic Energy (TKE) approach. The mixing length formulation varies with the spatial resolution of the simulation domain: Bougeault and Lacarrère (1989) at 2.5 km and at 1.25 km, and that of Deardorff at 250 m. 3D turbulent fluxes are computed for the last two domains (1.25 km and 250 m).

2.4. Surface model description

The four surface models allow to characterize each grid cell of the simulation domain by four different land covers (agricultural and natural land, urban areas, inland waters and sea or oceans). The surface schemes consist in Interaction between Soil Biosphere and Atmosphere (ISBA; Noilhan and Mahfouf, 1996) for agricultural and natural land, and two parameterisations of the Charnock (1955) formulation for inland waters, seas and oceans and Town Energy Balance (TEB; Masson, 2000), designed for urban and artificial surfaces. Finally, water, heat (radiation, conduction, convection), momentum and carbon dioxide fluxes between the Earth's surface and the atmosphere are aggregated according to the area fraction of the land covers within each grid cell. Within TEB, the urban landscape is simplified as a network of street canyons (Figure 3) of infinite length and equiprobable orientation. TEB simulates the exchanges of heat and water from three generic surfaces (road, wall, roof, Figure 3). In order to estimate microclimate within street canyons, TEB is generally used in conjunction with the Surface Boundary Layer (SBL) model which solves vertical turbulent diffusion within the average street canyon from the surface fluxes provided by the road, wall and roof (Hamdi and Masson, 2008; Masson and Seity, 2009). Off-line simulations with TEB have already demonstrated that TEB was able to accurately reproduce the energy balance of urban surfaces, the street air temperatures and the energy consumptions for a wide range of cities under various climates and seasons: Vancouver and Mexico (Masson *et al.*, 2002), Marseille (Lemonsu *et al.*, 2004), Basel (Hamdi and Masson, 2008), Łódź (Offerle *et al.*, 2005), Toulouse (Pigeon *et al.*, 2008) and Montréal (Lemonsu *et al.*, 2010).

TEB simulates the thermal functioning of a generic building (Figure 3): an energy balance is established on the outer surfaces of both wall and roof, taking into account the solar and infrared net radiation (Q*), the convective heat flux (Q_H), and the water evaporation (Q_E) for the roof. The evolution of the wall and roof internal temperatures (T_w and T_r, respectively) by heat conduction is then solved at each time step by the model. Finally, exchanges with the air inside the building are calculated from the air temperature inside the building (T_i). T_i is described in a simplified way to account for the inertia of buildings and the temperatures of the inner surfaces of walls and roofs (Masson *et al.*, 2002).

2.5. Baseline surface input data

The surface models require input data to estimate their parameters. The terrain for each simulation domain was described by Shuttle Radar Topography Mission data (SRTM), the spatial resolution of which is finer than those of the simulation domains described. Then, land cover types (urbanized fraction, fractions of natural or agricultural covers, freshwater and ocean) for the two domains with the coarsest spatial resolution (FR and IDF) were taken from the Ecoclimap database (Masson *et al.*, 2003). A specific database was developed by the Paris Urban Planning Agency (APUR) to characterize urban parameters necessary in TEB (Masson, 2000, for the necessary parameters) at 250 m spatial resolution (APUR, 2007). It was based on surface inventories and spatial analyses of the vector maps of buildings and parks and completed by the Scientific and Technical Construction Center (CSTB) for the radiative and thermal parameters of the materials.

Additional sources were needed for the estimation of anthropogenic fluxes for the City of Paris. An initial estimate of the heat flow generated by the road traffic within the street canyon was completed and incorporated in the surface parameterisation. Within each grid cell of the Paris domain, this heat flow was approximated by weighting the global heat flow generated by traffic within Paris (Colombert, 2008) by the fraction of road within the grid cell (normalized to the total fraction within the domain), and assuming that combustion of fuels generates 92% of sensible heat and 8% of latent heat, as postulated by Pigeon *et al.* (2007).

2.6. Modelling AC

2.6.1. Implementation of AC within TEB

In the baseline case (NO-AC), the indoor temperature within the TEB model evolves in a simplified way which accounts for the inertia of buildings and the temperatures of the inner surfaces of the walls. To

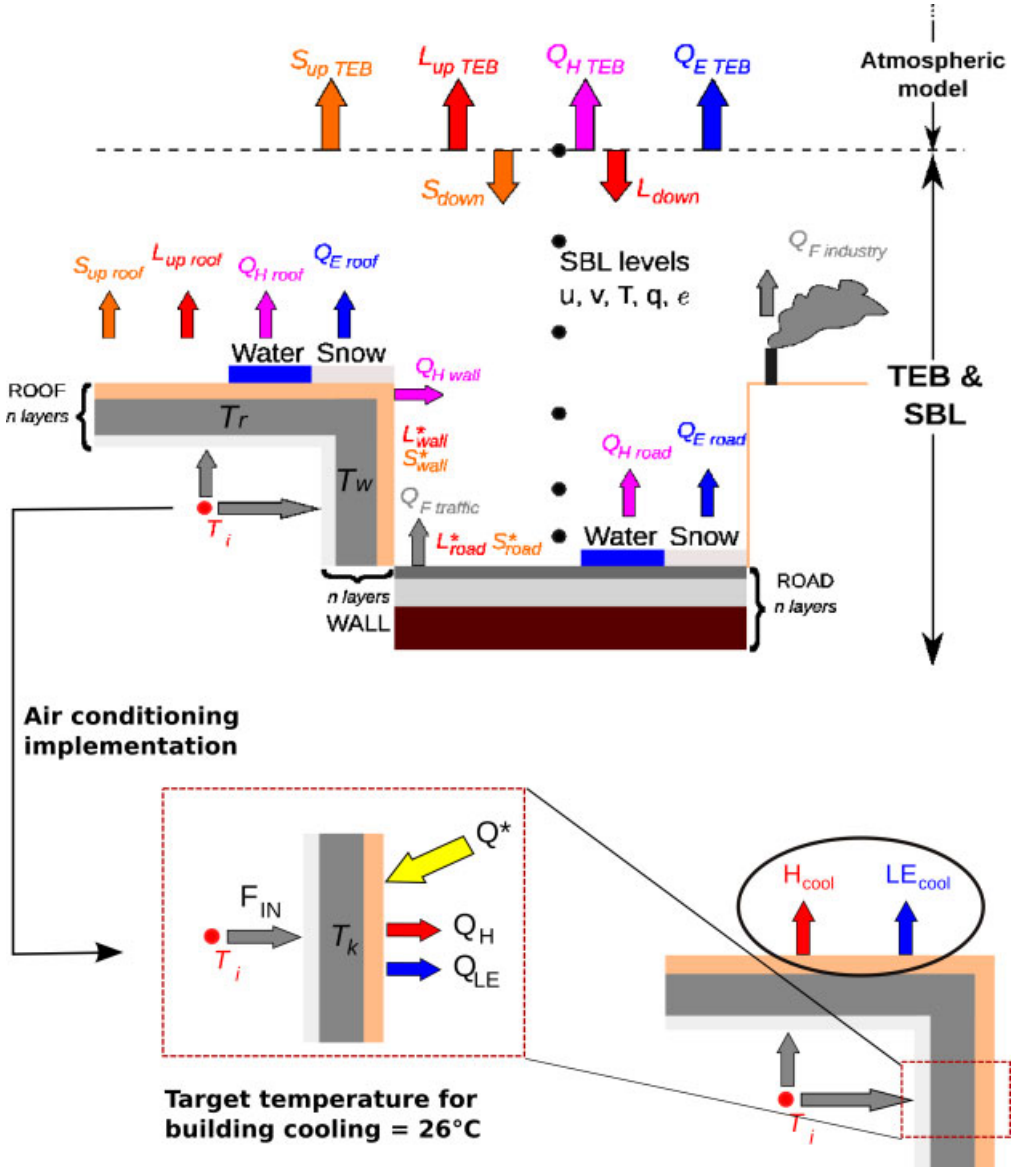

Figure 3. Schematic description of TEB model, showing how AC is accounted for at the building level. This figure is available in colour online at wileyonlinelibrary.com/journal/joc

Table II. Anthropogenic fluxes parameterisation within TEB.

Input data	Unit	Description
H_{cool}	W.m^{-2} of urban area	Maximum sensible waste heat flux associated with AC of buildings
LE_{cool}	W.m^{-2} of urban area	Maximum latent waste heat flux associated with AC of buildings
F_{cool}	–	Fraction of air conditioned buildings
$TIME_{cool}$(j,h)	–	Coefficients for the hourly modulation of the maximum AC waste heat flux, function of day type (j) and time of day (h)
T_{cool}	°C	Set-point temperature for air conditioned buildings

address the objectives of this study and account for AC usage, the TEB model has been slightly modified: the cooling of buildings has been represented by limiting the indoor temperature of air conditioned buildings to 26 °C (whereas, in the baseline case, there is no limiting of the indoor temperature), and by prescribing for those buildings the waste heat generated by air conditioners at roof level. The new surface data necessary for the model are presented in Table II. Two forms of AC waste heat released to the atmosphere are accounted for, which allow to describe common types of AC systems: sensible heat for dry cooling systems (H_{cool}, bottom diagram of Figure 3) and latent heat for evaporative cooling towers (LE_{cool}, bottom diagram of Figure 3).

This current implementation of AC within TEB, with a single setpoint temperature for air conditioned buildings and the integration of AC waste heat fluxes towards the energy balance of the roof, represents the cooling of buildings in a simplified way. Although 26 °C is a legal setpoint for comfort cooling, it is common knowledge, for example, that most luxury hotels in Paris apply an internal setpoint temperature below 26 °C, and frequently around 21 °C or lower. Also, some processes require much more cooling than required for comfort, as is the case, for example, with the food industry. Also, since the AC heat discharges to the atmosphere are currently prescribed to the model and not calculated from the cooling power demand of the buildings, it is not currently possible to model the retrofitting of the outdoor temperatures on the demand of cooling power in the buildings.

2.6.2. *AC current heat releases*

The AC systems currently used in Paris can be classified in four broad categories: (1) small dry cooling systems (from 6 to 70 kW per unit), (2) large dry cooling towers (for commercial centres, leisure facilities, data centres...); both systems discharge sensible waste heat to air, (3) evaporative cooling towers discharging latent waste heat to air, and (4) the free cooling plants (50 MW) developed by the Climespace Company discharging waste heat to the river Seine. These last two types of installations are mainly used for cooling large spaces, computer rooms, hospitals, and museums, or for cooling industrial processes, and are sometimes distributed via district networks such as those developed and maintained by the Climespace Company.

The estimation of the heat released by dry AC systems (1 and 2) over the Paris domain was undertaken based on a visual inventory via open-source satellite images for roof condensers and Google Street View for front condensers. The visual inventory of small condensers (1) was first carried out within inner Paris on a sub-sample of five districts (1, 11, 14, 16 and 18, Figure 2), representative in dwellings/businesses diversity and building type (building date, shape and allocation). The number and the cooling power of the small dry condensers observed yielded two levels of dry waste heat intensity for these five districts: 8 and 34 W m^{-2} of ground area. Each grid cell of the GP simulation domain was classified according to these two levels. Then, the waste heat associated with the large dry cooling towers (2) was added to each grid cell according to the number and the power of the installations observed during the visualisation phase. In terms of collating data for the evaporative cooling towers (3), their inventory was facilitated by the legal requirement imposed on them, as 'classified installations', to declare their power and other characteristics to the authorities due to the sanitary hazard that they might carry. The collation of their cooling power was obtained upon request from the 'Prefecture de département' (local authorities). In terms of heat discharge, the waste heat is assumed partitioned into 95% latent heat and 5% sensible heat. Finally, the heating of small corridors of the river Seine induced by the free cooling systems (4) was not integrated because the analysis of their temperature records (Climespace, personal communication) showed that they would not cause a significant impact on the temperatures of the lower layers of air above the Seine. Then, in addition to the sources of AC waste heat themselves, the thermal discharge of the power transformers supplying the AC systems was accounted for amounting to 3% of the electrical power requested by the AC systems identified.

Gathering the information from all the current sources of waste heat emission (AC systems and power transformers) resulted in the sensible waste heat fluxes (H_{cool}) and latent waste heat fluxes (LE_{cool}) presented on top of Figure 4 for the REAL-AC case. These stand for maximum values which are modulated by the hourly schedules provided in Figure 5, depending on the day of the week simulated. The hourly schedules of AC power demand for the period of simulation were gathered for each day type of the week (weekday, Saturday, Sunday) based on records from the Climespace Company, and then normalized. In conclusion, the inventory of AC waste heat releases for the REAL-AC scenario reports a waste heat power of 5.16 GW over the Paris domain and shows that sensible heat releases are more spread out than those of latent heat (Figure 4), which is consistent with the higher spatial density of small or large dry systems compared to evaporative cooling towers. Continuous zones present sensible heat releases of about 75 Wm^{-2} of urban cover area (top left of Figure 4), when higher values up to 650–900 Wm^{-2} occur locally. The highest values are located at powerful evaporative cooling towers connected to district networks and, in this case, a part of the cooling power generated is used in grid cells adjacent to where it is produced.

Then, from these data of waste heat release, the building surface and a median level of cooling power requirement, the fraction of cooled buildings in each grid cell was estimated. A cooling power of 90 Wm^{-2} of floor was chosen as being representative of a building fully air conditioned (median value for various building types such as offices in central Paris, offices with data centres or IT department, shops and malls, with 100% of air cooled floor area). Consequently, the fraction of air conditioned buildings (F_{cool}) was calculated as follow for each grid cell.

$$F_{cool} = \min\left(\frac{\dfrac{H_{cool} + LE_{cool}}{BLD \times \dfrac{z_{BLD}}{2.5}}}{90 \times \left(\dfrac{1 + COP}{COP}\right)},\ 1\right)$$

where BLD is the grid cell average building plan area density of the urban area, z_{BLD} is the grid cell average building height, COP is the Coefficient of Performance taken as 2.5 and the floor-to-floor height is fixed at 2.50 m. Then the waste heat fluxes estimated for the

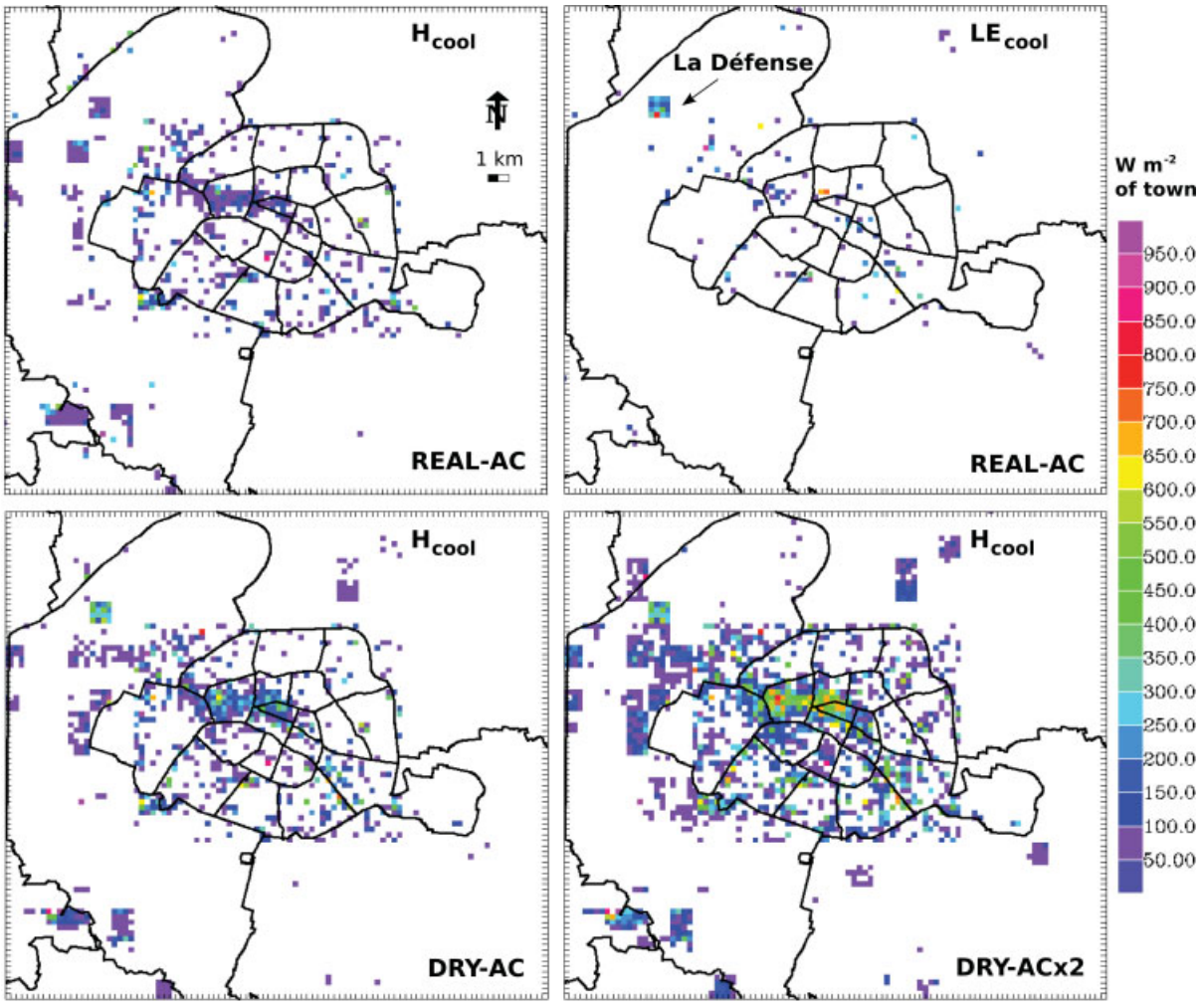

Figure 4. Maximum AC waste heat fluxes for the three scenarios with heat discharges to air Top: REAL-AC scenario, sensible heat fluxes (left) and latent heat fluxes (right) Bottom: DRY-AC scenario sensible heat fluxes (left), DRY-ACx2 scenario sensible heat fluxes (right).

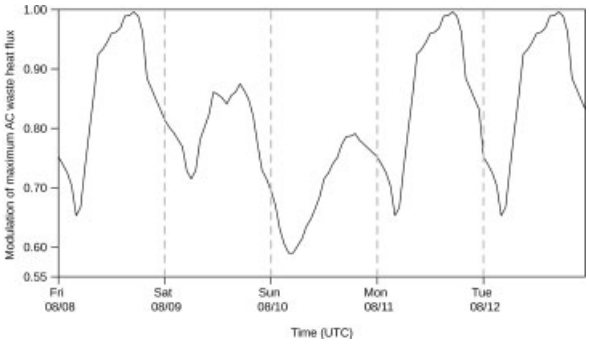

Figure 5. Hourly schedule for the modulation of maximum AC waste heat fluxes based on records from the Climespace Company.

REAL-AC case served as a basis for the development of the waste heat fluxes for the remaining AC scenarios (Table I).

2.6.3. *AC scenario heat releases*

The maps of heat fluxes for the two AC scenarios discharging only dry waste heat to air (bottom maps on Figure 4) were developed by converting the latent heat released by evaporative cooling towers or free cooling installations to sensible heat. Moreover, in the case of cooling installations connected to the district network, the sensible heat releases have been attributed to the grid cells where the cooling power is used. A good example of the consequences of the relocation of those waste heat discharges at the level of the cooled buildings is the office district of 'La Défense' (Figure 4, REAL-AC and DRY-AC scenarios). Also, a ratio of 1.05 was used to convert latent heat discharges to sensible heat, assuming a drop in the COP value between evaporative cooling towers and small dry systems. This drop has been observed by the Climespace Company and occurs because the dry autonomous systems have generally a lower-level performance by construction, and a lower level of monitoring and maintenance. By comparison, the large evaporative cooling towers, or free cooling plants that distribute their cooling power by district network, are monitored and adjusted around the clock to have the best level of performance. For the DRY-ACx2 scenario, the heat discharge power over the Paris domain was doubled (10.32 GW) to be consistent with the forecasts by Adnot (2003a, 2003b) predicting by

2020 an increase in commercial and office surfaces in France such that it would induce about a doubling of the AC consumption in comparison to 2003 (mean across 11 AC technical scenarios, Adnot, 2003b). Two thirds of this increased AC power was distributed in central Paris (on the hypothesis that the increase in commercial and business surfaces would occur there) and one third outside. In this scenario and the NOAIR-ACx2 scenario, F_{cool} has been recalculated to represent this increase in cooled buildings.

2.6.4. Uncertainties and limitations

The accuracy of the current heat release inventory (REAL-AC case) has been evaluated. Firstly, to assess the quality of the visual inventory, the cooling power values have been recovered for a set of ten buildings (mostly hotels within inner Paris). For the buildings of this set for which the condensers have been visualized, the uncertainty has been estimated to be 15%. For some buildings, although present, the systems had not been visualized because they were placed on the inner facet of the building, hidden within a compartment, the attic or the basement. The global result of the visual estimation for this set of ten buildings in comparison with the real consumption was an underestimation of the heat releases by a factor of two.

Secondly, concerning the accuracy of the releases by the classified installations (evaporative cooling towers), it did not prove to be feasible to collate data for all installations in Greater Paris. This study was based on a record of 1740 classified installations out of 2118 (i.e. 82% of operating installations).

3. Evaluation and analysis of the baseline simulation

3.1. Evaluation against meteorological observations

The baseline simulation without AC has been evaluated against meteorological observations to establish how well the configuration of the coupled models behaves in the context of this study. For this purpose, we used the temperatures simulated at 2 m for the vegetated fraction of each grid cell in order to be consistent with the temperatures provided by weather stations which are measured on a grassy area away from any obstacle (hence, generally in parks in urban settings). In the case of the IDF domain, there are 31 stations providing hourly records of temperatures. On the other hand, rare are the urban weather stations recording hourly temperatures. In the case of Paris, there are five. Their location is shown on the bottom of the map in Figure 2. Two stations are located in inner Paris: Paris-Montsouris (P-M) within the Park Montsouris, south of the river Seine and Belleville Park (B-P). The other three are located outside inner Paris: southwest of Paris for Villacoublay (V) at the military airport, northwest of Paris for Courbevoie (C) and north of Paris for Saint-Denis (S-D). Figure 6 presents the evolution of the 2-m temperature modelled during the heat wave at a 1.25 km resolution for the 31 weather stations of the IDF domain (top left), and at a 250 m resolution for each of the five weather stations of the GP domain. At 1.25 km horizontal resolution, the standard deviations for simulated temperatures are lower than those observed for daily minima (top left of Figure 6), showing that the model, at this resolution, underestimates the geographic variability of daily minima. Nevertheless, the model is able to properly simulate the evolution of daily temperatures at the scale of the IDF. On average, the model is slightly too cold during the day and too warm at night (Table III). This tendency of the model to overestimate the daily minima is also observed across the GP domain, but to a lesser extent because the increase in resolution (from 1.25 km down to 250 m) shows a better correlation between simulated and observed 2-m air temperatures (Table III). This improved correlation is characterized by a root mean square error (RMSE) on the 2-m temperature of 1.5 °C for the GP model compared to 2.6 °C for the IDF model, with respective mean bias errors (MBE) of 0.2 °C and 1.0 °C. Increasing in resolution, the prediction of minimum temperatures is the most improved, with a RMSE of 1.3 °C for the GP domain *versus* 3.5 °C across the IDF domain and respective MBE of 1.0 °C and 3.0 °C. The prediction of the maximum temperatures remains relatively unchanged when changing resolution, with an average RMSE and MBE of 1.7 °C and −0.2 °C. These improvements are attributable not only to the spatial resolution itself, but also to a better description of the different types of surface covers on the GP domain.

The RMSE and the MBE were also calculated for the REAL-AC scenario as this is the scenario closest to reality. They were equivalent to those estimated for the baseline simulation. Indeed, there are not enough stations within the GP domain and they are not located near enough to substantial sources of AC waste heat emissions to demonstrate a better agreement between the temperatures simulated and observed when current AC waste heat emissions are accounted for.

The evaluation of the simulation on the FR domain against meteorological observations is presented in Appendix A.

3.2. Characteristics of the baseline UHI

The description of results from the NO-AC scenario is of importance as it sets a baseline for further comparison, as the model results are analysed in terms of differences (temperature anomalies). This enables, over the Paris domain, not only to compare the impacts of AC scenarios with the baseline situation, but also to free oneself from the remaining bias between the modelled and the observed temperatures. Figure 7 presents a map of 2-m air temperatures as well as a 2-m air temperature profile obtained for a west-to-east cross-section passing through the hottest districts of inner Paris. This profile is used to visualize with a finer scale of temperature the structure of the heat island for that cross-section, and to refine the magnitude of the heat island in the direction indicated.

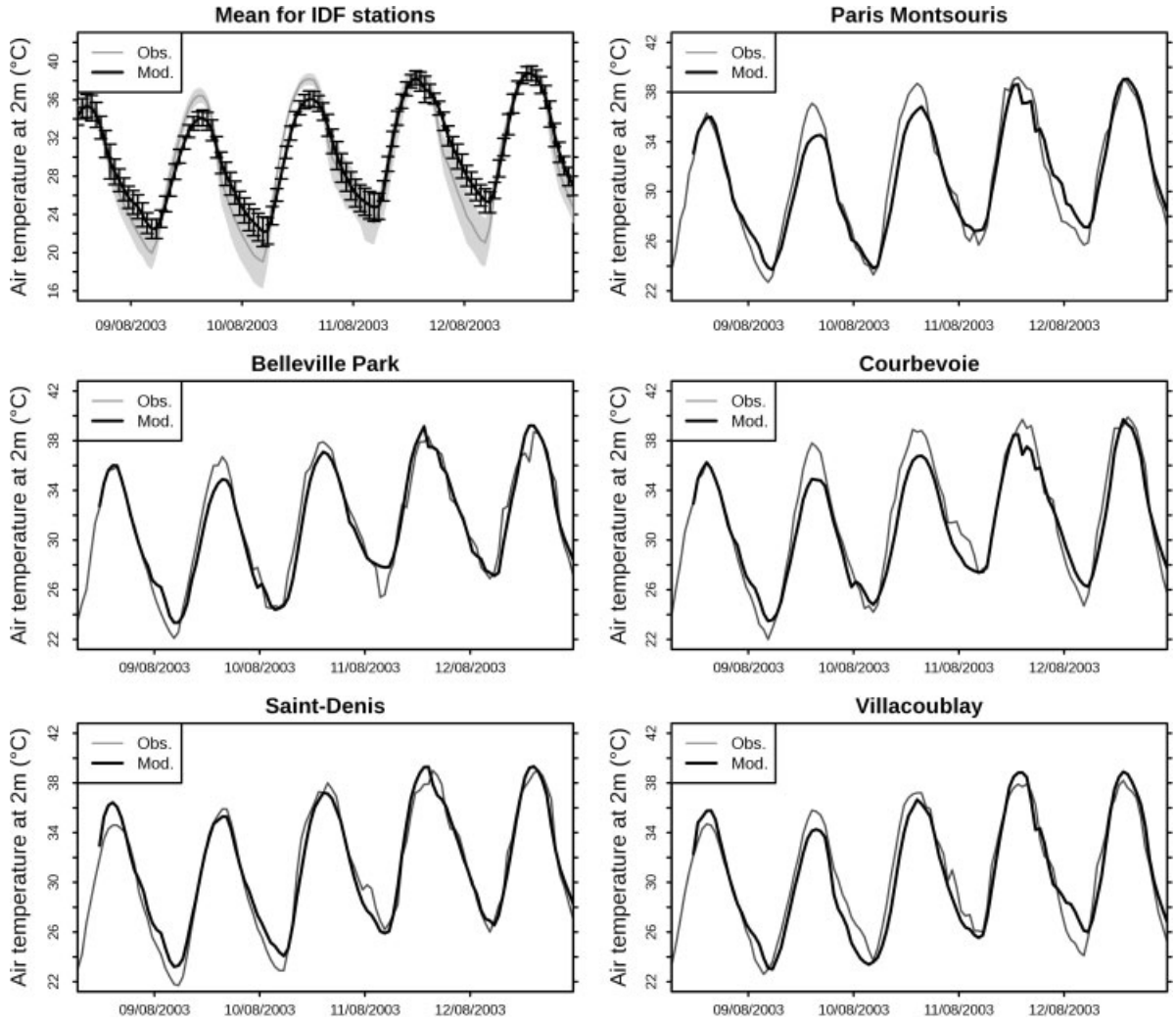

Figure 6. Temperatures observed and modelled between 8 and 12 August 2003, for IDF weather stations (top left: full lines represent the mean across 31 stations; standard deviations are indicated by whiskers for the model and by a grey envelope for observations) and for each of the five Greater Paris stations.

Table III. Root Mean Square Error (RMSE) and Mean Bias Error (MBE) Mod-Obs on 2-m air temperatures, calculated between 8 August 2003, 12 UTC, and 13 August 2003, 23 UTC, based on the maximum number of weather stations in each domain (31 for IDF and 5 for GP).

Domain/Spatial resolution	T (°C)		Tmin (°C)		Tmax (°C)	
	RMSE	MBE	RMSE	MBE	RMSE	MBE
IDF/1.25 km (for 31 stations)	2.6	+1.0	3.5	+3.0	1.9	−0.5
GP/250 m (for 5 stations)	1.5	+0.2	1.3	+1.0	1.6	+0.1

The mean nighttime 2-m air temperatures present the structure of a standard UHI (Figure 7), which demonstrates the influence of the most urbanized areas in central Paris on the temperatures. Its maximum amplitude (between the hottest districts 2, 3, 9 and 10) and the least urbanized areas in the southwest of Paris) is about 6 °C. The mean nighttime temperature profile for the west-to-east cross-section passing through the districts 8, 9 and 10 (bottom of Figure 7) shows finer temperature variations and, in particular, the influences of artificial and natural surfaces on temperatures, with the highest temperatures over the densest urbanized areas (between 8 and 15 km) and lower temperatures over the Bois de Boulogne (between 6 and 8 km), and the river Seine (at approximately 3.5 km). The temperature profile shows a baseline UHI amplitude of about 4.5 °C, which can stand as a reference for assessing the potential impacts of AC scenarios on UHI. The UHI amplitude was estimated as the difference between the maximum of the mean nighttime temperature profile and the average of its two minima (east and west of the cross-section). The value of 4.5 °C agrees well with that of 4 °C observed

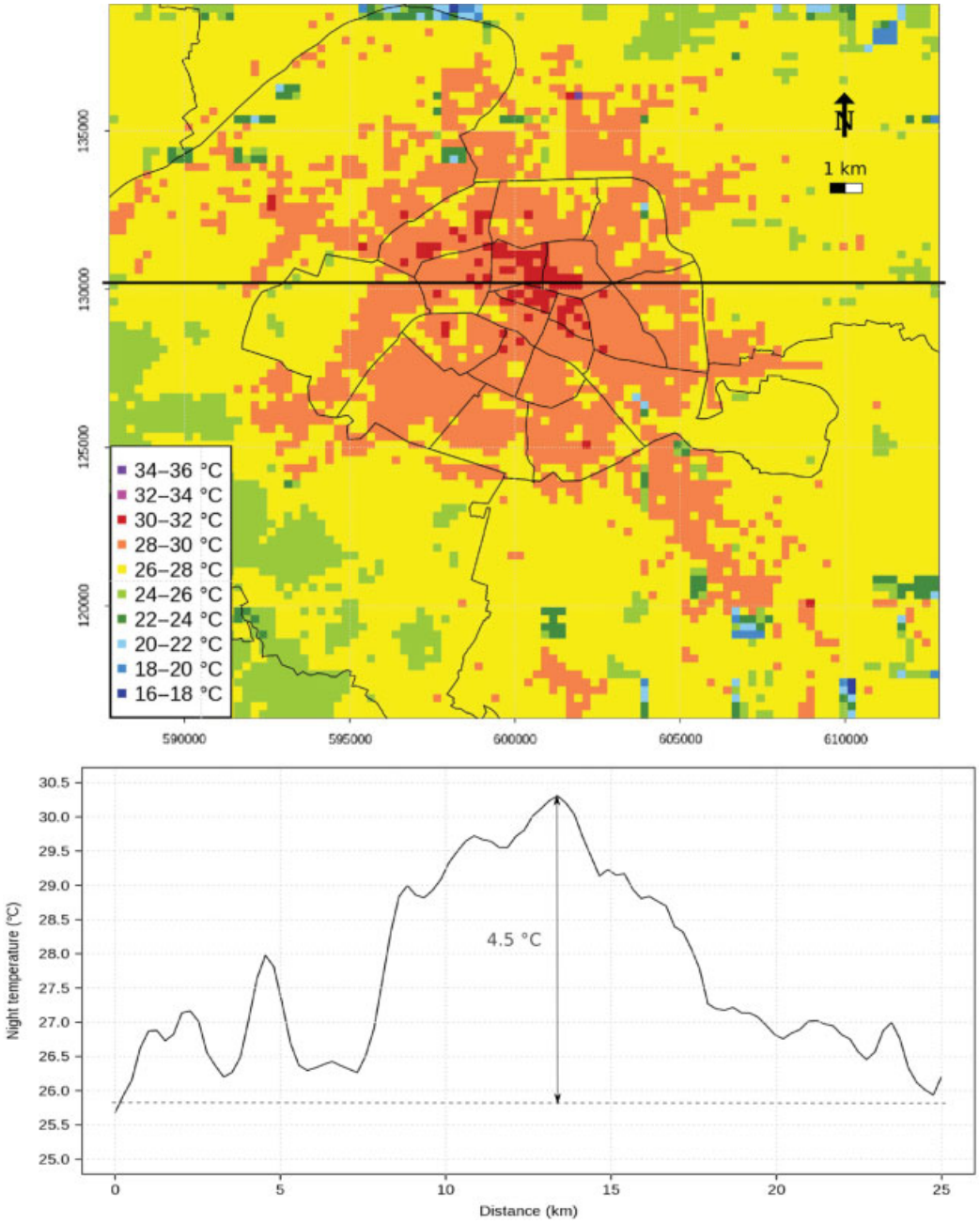

Figure 7. Characteristics of Paris nighttime UHI without activation of air conditioning (top: map of temperatures; bottom: mean temperature profile for the west-to-east cross-section mentioned on the top map, estimated across three hourly terms – 2, 3 and 4 UTC). The amplitude of the heat island is estimated on the temperature profile as the difference between the maximum and the average of the two minima (east and west).

during the 2003 heat wave between the city centre and the limit of the dense agglomeration of Paris.

4. Results and discussion: analysis of the AC scenarios

4.1. Statistical processing to estimate the impacts of AC scenarios

Potential impacts of AC have only been analysed for the Paris simulation domain where it was parameterized in the model. We have chosen two indicators to compare the differences between each AC scenario and the baseline scenario, both based on street air temperatures. Firstly, we have estimated the differences in 2-m street air temperatures between each scenario and the baseline over the simulation period, and it is called the 'temperature anomaly'. Secondly, we have compared urban heat islands morphology (maps) and amplitude (maps and temperature profiles) between all the scenarios.

Prior to the analysis, the temperature anomaly time series within each grid cell were processed in three steps using the R tool (R Development Core Team, 2010). Firstly, the filtering of anomaly time series was necessary to remove some storm-type events that have

occurred during the period as described in Section 2.2 and Appendix A. Indeed, in the simulations for which only the AC heat releases have been changed, some storm-type events have appeared at different locations and timings between two cases and have generated impacts on air temperature. However, given the current state-of-the-art in storm prediction, the perturbations of deep convection between two different simulations can grow rapidly (Hohenegger and Schär, 2007), and it is not possible to attribute these storm pattern modifications to the AC heat releases. Secondly, a random resampling of filtered anomalies by daytime (9 a.m.–7 p.m.), and nighttime (8 p.m.–6 a.m.) series was necessary so as to (1) obtain uncorrelated data, and (2) generate for each grid cell a larger sample that would follow a quasi-normal distribution before proceeding to anomaly characterisation. This resampling was performed using a bootstrapping method (Efron and Tibshirani, 1993). Thirdly, the characterisation of daytime and nighttime anomalies was based on a one-sided statistical test at 95% confidence on the average of the filtered and resampled daytime and nighttime temperature anomaly series to rank them in relation to fixed temperature thresholds.

To analyse the morphology and the amplitude of Paris mean UHI for each simulation, the 2-m temperatures for three nighttime hourly terms (2, 3 and 4 UTC) and the last four nights of the simulation (9–10, 10–11, 11–12 and 12–13 August) were selected and averaged.

4.2. Impacts of AC scenarios on street level air temperatures

Figure 8 shows the location and the amplitude of the daytime and nighttime temperature anomalies obtained for each of the four scenarios with AC (REAL-AC, DRY-AC, DRY-ACx2, NOAIR-ACx2). These results highlight four main outcomes.

4.2.1. Increase in street air temperatures

Firstly, all AC scenarios, but the NOAIR-ACx2, show an increase in street air temperatures, and the amplitude of this increase varies with the scenario of AC waste heat emission considered and the time of day. Under the present time REAL-AC case, 2-m air temperature anomalies range from 0.25 to 1 °C locally (across a grid cell, i.e. at 250 m), with the greatest temperature anomalies (1 °C) observed in districts 8 ('Etoile'), 12, 13 and 14 ('Montparnasse') for grid cells which are strongly air conditioned. Moving on to the DRY-AC scenario shows increased impacts, ranging from 0.25 to 2 °C. In this scenario, temperature anomalies of at least 0.5 °C are widespread in districts 2, 8 and 9 and 'La Défense' office district, and can be up to 1 and 2 °C locally (e.g. for the 'Etoile' and 'Montparnasse' neighbourhoods, in districts 8 and 14, respectively). Under the DRY-ACx2 scenario, impacts are even greater than for the DRY-AC scenario, ranging from 0.25 °C to 3 °C locally, with the greatest anomalies found in districts 2, 8 and 9. For these three AC scenarios, the increase in street air temperature is generally greater near the sources of emission of AC waste heat (shown in the maps of waste heat fluxes in Figure 4). It should also be noted that impacts of AC on local air temperatures in the area of 'La Défense' office district (northwest outside inner Paris, see Figure 8) only appear clearly with the DRY-AC and the DRY-ACx2 scenarios, due to converting latent heat releases from the REAL-AC scenario to only dry releases (heat fluxes in Figure 4).

Moreover, the uncertainty carried by the inventory of AC waste heat intensities over Greater Paris for the REAL-AC case (Section 2.6.4) suggests that the impacts on street air temperatures of the AC scenarios simulated estimated in this study are likely to be underestimated.

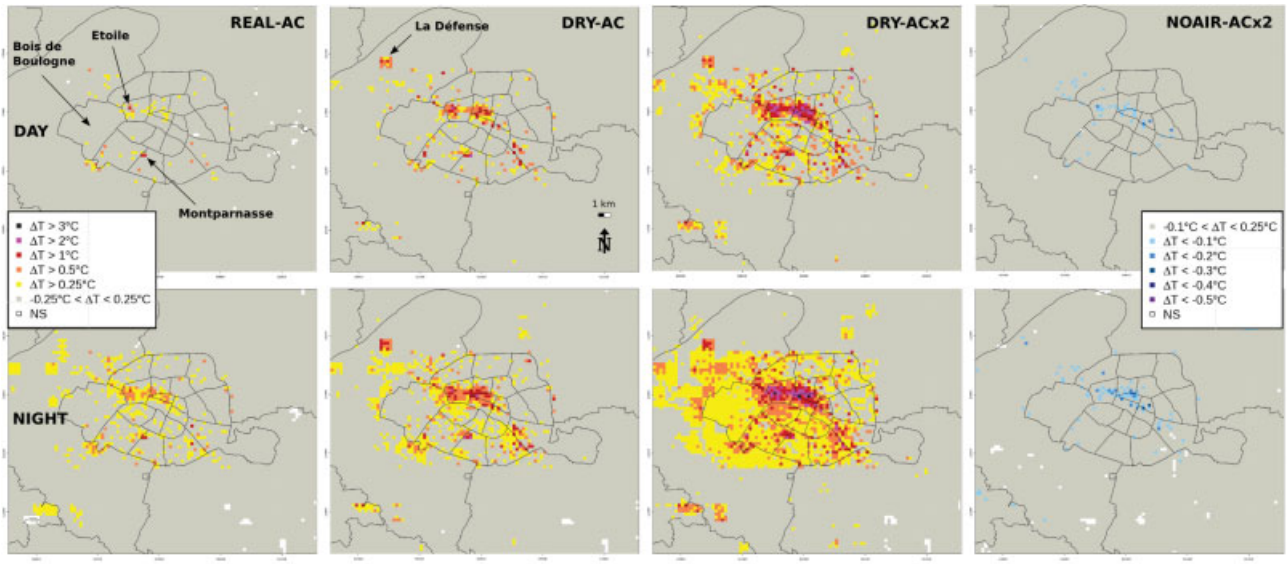

Figure 8. Street level (2 m) air temperature anomalies estimated at daytime (top) and nighttime (bottom) between 8 and 13 August 2003 for each scenario with air conditioning (by reference to the baseline/NO-AC scenario). Temperature anomalies were obtained through a random resampling of simulated temperature anomalies (from 9 a.m. to 7 p.m. daytime, and from 8 p.m. to 6 a.m. night time) and a one-sided statistical test at 95% confidence. NS stands for non-significant temperature anomalies.

Nevertheless, at the scale of Paris City, the magnitude of the impacts of the AC scenarios discharging waste heat to air corroborates relatively well with the results from Kikegawa *et al*. (2003) and Ohashi *et al*. (2007) obtained at the scale of Tokyo office districts, showing an increase in street air temperatures of 1 and 1–2 °C, respectively. Hsieh *et al*. (2007) for Taipei's densest residential district, demonstrated a similar increase in street air temperature of between 0.78 and 1.84 °C.

Results for the NOAIR-ACx2 are of a different nature: they present temperature anomalies which are negative, meaning that this scenario has a potential for cooling the streets. However, the activation of AC within the buildings did not reduce the street air temperature by more than 0.2 °C during the day.

4.2.2. *Greatest impacts at night*

Secondly, AC is used more during the day (when it is the hottest) than during the night (Figure 5). However, the impacts on local air temperature are the strongest at night and all the AC scenarios with heat discharge to air show an increase in street air temperatures that is greater at nighttime than daytime (first three scenarios, left of Figure 8). Why is this? In fact, this common characteristic is consistent with, and can be explained by, a different structure of the atmospheric boundary layer at nighttime and daytime. The vertical profiles of simulated potential temperatures presented in Figure 9 for the DRY-AC and the DRY-ACx2 allow to estimate the depths of the mixing layer at different times of the day (based on Sullivan *et al*., 1998). The large boundary layer thickness of about 2300 m observed throughout the day, correlated to a strong turbulent mixing, explains the low amplitude of temperature anomalies observed during the day. At night, due to the thinness of the boundary layer (about 250 m, Figure 9) and the much lower turbulent mixing, the impacts of heat releases on temperature are greater than those observed during the day. These processes can explain the greater anomalies observed at night for some grid cells, as well as the occurrence of temperature anomalies at night where they did not exist during the day (areas with 0.25 °C anomalies). For example, for the DRY-ACx2 scenario, temperature anomalies observed during the day range from 0.25 to 2 °C (Figure 8). At night, they can reach up to 3 °C locally and wide areas with a 0.25 °C anomaly appear. Under this scenario, districts 2, 8 and 9 again show the strongest impact at nighttime (1–2 °C in almost all the grid cells concerned). The appearance at night of areas with a 0.25 °C anomaly is also the case with the DRY-AC scenario but to a lesser extent (Figure 8). Besides, it may be noted that the impacts on temperatures observed at night for the DRY-AC scenario are equivalent to those for the DRY-ACx2 during the day (both in terms of amplitude and spatial extent). This can again be explained by Figure 9 which highlights similar depths of the mixing layer for the DRY-AC and the DRY-ACx2 scenarios, whether at nighttime or daytime (around 250 m at nighttime, and 2200 and 2350 m at daytime, respectively), and therefore explains why, with greater waste heat releases in the DRY-ACx2 than in the DRY-AC, the DRY-ACx2 presents greater temperature anomalies than the DRY-AC (Figure 8).

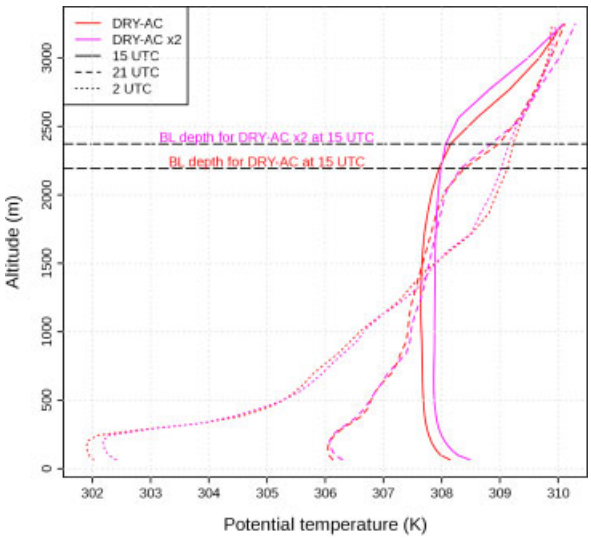

Figure 9. Vertical profile of potential temperature (averaged across a 2.5 × 2.5 km^2 zone centred on the west-to-east cross-section shown in Figure 7) for the DRY-AC and the DRY-ACx2 scenarios, on 10/08/2003 15 and 21 UTC and 11/08/2003 2 UTC. This figure is available in colour online at wileyonlinelibrary.com/journal/joc

In the case of the NOAIR-ACx2 scenario, the temperature reduction is also slightly more pronounced at night than during the day (for a few grid cells, the temperature reduction has improved by 0.1 °C), although still less than 0.5 °C (bottom right of Figure 8). These impacts remain marginal and we can not conclude that this scenario, which constitutes an attempt to mitigate AC impacts on the urban climate, would allow to substantially cool the streets of inner Paris (and, consequently, reduce the UHI) in addition to cooling the buildings. The slight cooling effect observed might not be perceptible or beneficial to the inhabitants.

4.2.3. *Variable extent of AC scenario impacts*

Thirdly, while the impacts on temperature in the REAL-AC case are relatively localized by or near the sources of release of AC waste heat, in the DRY-AC, the grid cells which are heavily air conditioned start to affect slightly adjacent grid cells (Figure 8). Indeed, with this latter scenario are emerging wide zones of several grid cells bearing temperature anomalies of 0.5 °C even during the day (in districts 2, 8, 9 and 'La Défense' office district). The comparison of these two scenarios (REAL-AC and DRY-AC) shows that assigning the sources of heat emission locally to user buildings (DRY-AC) instead of centralising them to a cooling production unit (as is the case when buildings are connected to a cooling network in the REAL-AC case) does have an effect, however limited, on the spatial spread of the temperature increase at the scale of the city. Our results suggest two factors that generate a significant spatial extent of impacts.

The first one is the nighttime situation (explained just above) since during the night more grid cells presented significant temperature anomalies than during the day (areas with anomalies above 0.25 °C for example). The second one is the intensity of AC heat discharge. Indeed, contrary to the DRY-AC scenarios, the DRY-ACx2 impacts wider zones in the city, with repercussions on the temperature that extend beyond the areas where the heat emissions are prescribed (west of Paris, including the 'Bois de Boulogne' and further, Figure 8) and larger zones bearing 1 °C temperature anomalies at daytime and 2 °C at nighttime. In summary, the thermal impact of heavily air conditioned grid cells on surrounding grid cells is gradually increasing at night and with the intensity and the type of heat discharge (first three AC scenarios from left to right in Figure 8).

4.2.4. Greatest impacts of dry systems

When analysing the previous results by focusing on the type of AC systems simulated (air-cooled *versus* water-cooled), it appears that the scenarios that evaluate the equipment of the city with only dry and individual AC systems (DRY-AC and DRY-ACx2) generate the greatest increase in temperature, both in terms of amplitude and spatial extent. This suggests that a conversion from water-cooled to air-cooled AC systems would not be a sustainable option in terms of street temperatures and, therefore, energy demand.

4.3. Impacts of AC scenarios on Greater Paris heat island

The urban heat islands for each AC scenario are analysed in the form of maps (Figure 10) and temperature profiles (Figure 11) which are compared to those of the baseline NO-AC scenario (Figure 7). Given the results obtained for street level temperatures, remarkable trends have been observed for the nighttime UHI. Figure 10 illustrates well the variations in the spatial structure of the heat island between the scenarios with AC and the baseline (Figure 7). Although the heat islands diagnosed for each scenario retain a standard UHI structure, the heat island simulated for the AC scenarios with heat release to air present a spreading of the hottest areas in central Paris compared to the baseline scenario. This spreading is gradual from the REAL-AC case to the DRY-AC and the DRY-ACx2 scenarios. A clear amplification of the heat island appears with the future projections of waste heat emissions of the DRY-ACx2 scenario. The maximum amplitude across the Paris simulation domain reaches approximately 8 °C, which corresponds to a 2 °C increase compared to all the other scenarios (Figures 7 and 10). District 8 of inner Paris seems to be the most affected by the gradual spreading and amplification of warmer

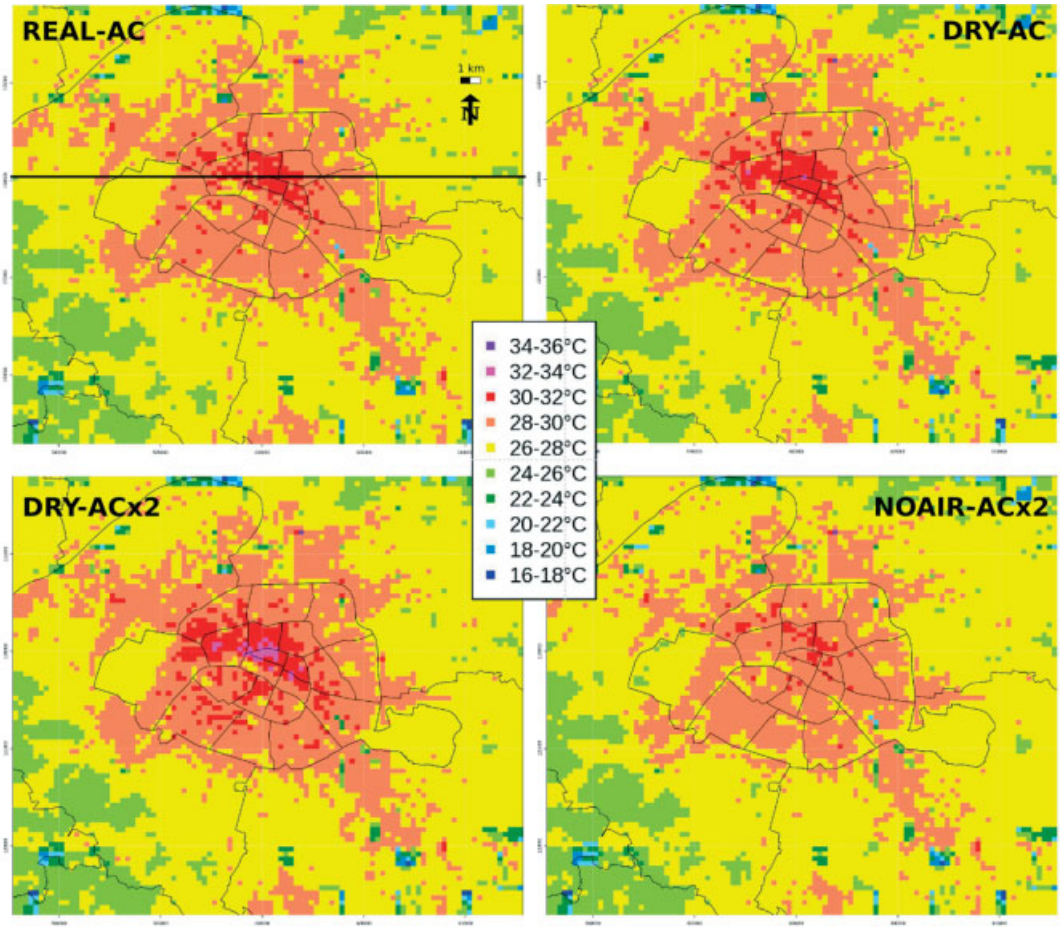

Figure 10. Comparison of the UHI generated by the four air conditioning scenarios.

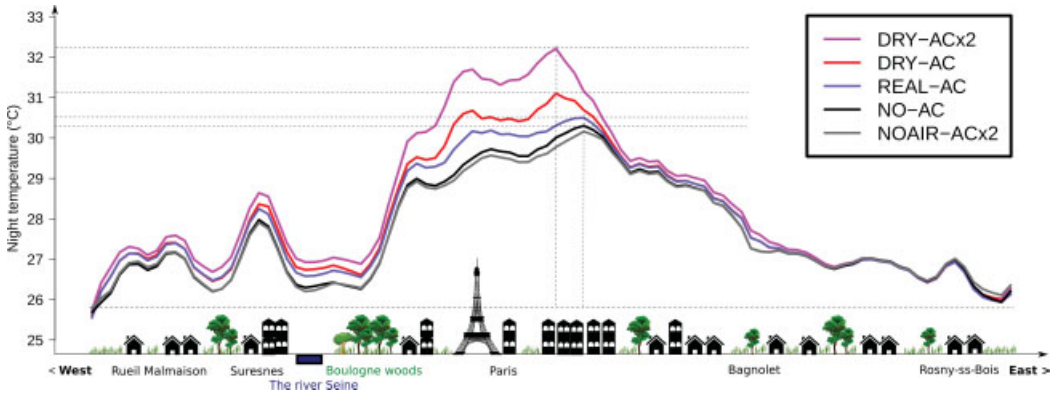

Figure 11. Temperature profiles showing Paris UHI for a west-to-east section passing through the warmest districts of inner Paris (8, 9 and 10, as shown by the black line in Figure 7 for the NO-AC scenario).

temperatures. As expected, the heat island diagnosed for the NOAIR-ACx2 scenario presents a much less spread-out structure of the warmest areas than the baseline NO-AC scenario.

Looking at the temperature profiles (Figure 11), the increase in waste heat logically resulted in an increase in the magnitude of the urban heat island. Indeed, compared with an amplitude of 4.5 °C in the baseline NO-AC scenario (bottom of Figure 7 and dotted lines reported in Figure 11), scenarios with AC heat releases to air show a steady increase in UHI amplitude with a value of 4.8 °C for the REAL-AC case, 5.3 °C for the DRY-AC scenario, and 6.4 °C for the DRY-ACx2 scenarios.

5. Conclusions and perspectives

Compared with pre-cited studies on the impact of AC on temperatures at the scale of neighbourhoods, this study, by coupling an urban energy balance model to a meso-scale atmospheric model, has allowed to access the impact of AC on temperatures at the scale of a city. This study was conducted to compare, for the City of Paris, different systems and intensity of cooling power to meet the chilling requirements inherent to some buildings now and in the near future. Our results suggest that the classic means to meet the cooling needs of the buildings in Paris during a heat wave event similar to that of 2003 are likely to increase street air temperatures and, consequently, the amplitude of the heat island, with the most intense impacts near the greatest AC waste heat releases. The impacts observed on street air temperatures varied with the type of AC systems and the intensity of emission simulated, but the proliferation of dry systems demonstrated the greatest increase in street air temperatures and the worst enhancement of the nighttime heat island. All the systems releasing waste heat to air showed an increase in street air temperatures in the most urbanized parts of central Paris, of 0.5 °C considering the current AC equipments (with reference to 2003), of 1 °C if all current systems were replaced by dry autonomous AC systems, and 2 °C in case Greater Paris was led to double its cooling load. And these impacts have probably been underestimated because of the uncertainty in the inventory of waste heat from air conditioning systems. Finally, the impact of a future situation with a large number of air-cooled buildings without generating waste heat to the air lowered street air temperatures but not significantly enough to be perceptible by the inhabitants. Besides, if the free cooling systems were to be generalized at the scale of the entire city in the future, the impacts of the warming up of the river Seine (due to this cooling technique) on air temperatures should be studied with caution.

This study shows that future developments of cooling facilities at the scale of a city like Paris should preferably be controlled so as to be sustainable. Besides, the increase in temperature observed for most of the AC scenarios bears consequences, not only in terms of energy consumption, but also regarding public health. Our simulations showed the greatest increase in temperature at nighttime, which might exacerbates night thermal stress (for those without access to AC), a factor identified in Paris as highly related to excess mortality during the 2003 heat wave (Ledrans *et al.*, 2005; Dousset *et al.*, 2011). In terms of energy, the increase in temperatures related to the usage of AC is likely to lead to an increasing demand for air cooling (and, consequently, energy consumption), while at the same time lowering the efficiency of air conditioners. But in order to study these feed-back processes, the urban energy model TEB will need to be improved. To provide an energy balance for the buildings that would be not only more consistent with the observations but also dynamic, the new version of TEB will calculate the evolution of the internal temperature of buildings by an energy balance equation that will account for heat gains such as the internal loads of the building (corresponding to people, uses of energy for lighting and various electrical needs) and the direct solar gain through glazing, as well as the representation of the building internal thermal mass (floors and load-bearing walls). These implementations will allow for calculating AC waste heat emissions in relation to the demand for cooling within the buildings (i.e. in relation to outdoor temperatures). These developments will also allow to run simulations for cities which do not have access to AC waste heat records. Future work

will as well focus on simulating the combined impacts of AC on temperature and humidity, which is of importance for humid cities, but was not the case for the 2003 heat wave in Paris.

Acknowledgements

The results presented in this publication are the outcome of the CLIM^2 project which was co-funded by the CNRM-GAME (Météo France and CNRS) and by the Climespace Company. This work has benefited from the expertise developed within the multidisciplinary study EPICEA, a study on the impacts of climate change at the scale of Greater Paris, which was funded by the City of Paris as part of its Climate Action Plan. We would especially like to thank Aude Lemonsu (CNRM/GAME), Raphaëlle Kounkou-Arnaud and Julien Desplat (DIRIC – MétéoFrance), Julien Bigorgne (APUR) and Jean-Luc Salagnac (CSTB).

Appendix A

A1. Model configuration and evaluation on FR domain

The sporadic and very localized storms that occurred during the simulation period are not easy to simulate, hence several configuration versions were tested for the model running over France (parent model for the three-nested model configuration) in order to improve the consistency between the simulation results and the hydrological situation.

Two main configurations were tested: one with a deep convection scheme activated (DCS; Kain and Fritsch, 1993) running at a 6 km spatial resolution, and one with a cloud-resolving model (CRM, with a 2.5 km spatial resolution). In both configurations, surface parameters were initialized and coupled with the reanalysis of the numerical weather prediction system of the European Center for Medium Range Weather Forecast.

Test results showed that the DCS configuration running at 6 km resolution generated excessive precipitation. For the CRM configuration running at 2.5 km resolution, even though precipitation was on the whole better simulated than in the DCS configuration in terms of location, the accumulated precipitation was still too high compared to observations. In both cases, the overestimation of precipitation was attributed to high soil moistures, which was not consistent with the soil drought conditions observed over that period of time. Consequently, for the two configurations, initial soil moisture conditions were adjusted over the entire domain by uniformly initialising soil moisture with a soil water content index of 0.2. This uniform value was chosen based on the reanalysis of soil moistures by Météo France for the beginning of August 2003 (SAFRAN-ISBA-MODCOU data (SIM), Habets *et al*., 2008). Adjusting soil moisture in the DCS configuration did not significantly improve the simulation of precipitation, which remained too abundant (up to around 35 mm locally) and far too spread out compared to those observed (Figure A1), demonstrating the inability of that specific parameterisation to reproduce sporadic storms during the heat wave. On the contrary, the adjustment of soil moisture to that of SIM improved the simulation of precipitation by the CRM configuration (Figure A1), showing that this configuration was well able to reproduce the patterns of precipitation at the scale of the entire domain, mainly in terms of extent, with daily accumulation locally up to about 35 mm (Figure A1).

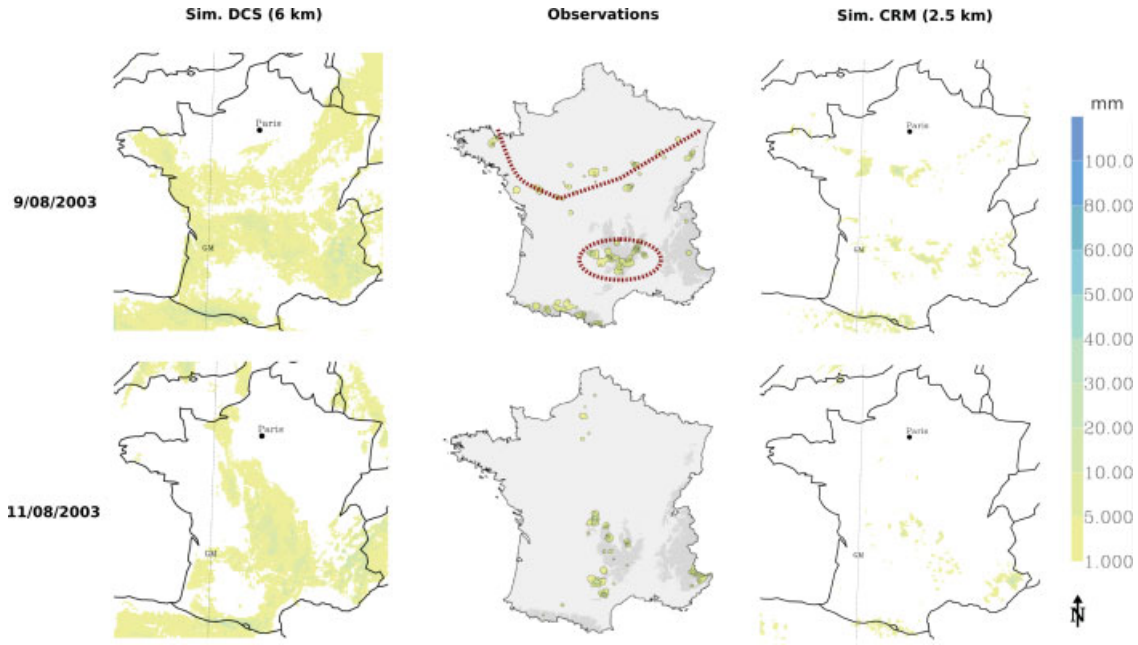

Figure A1. Accumulation and location of precipitation observed on FR domain (centre) and simulated at a 6 km (left) and a 2.5 km (right) spatial resolution, for 9 and 11 August 2003.

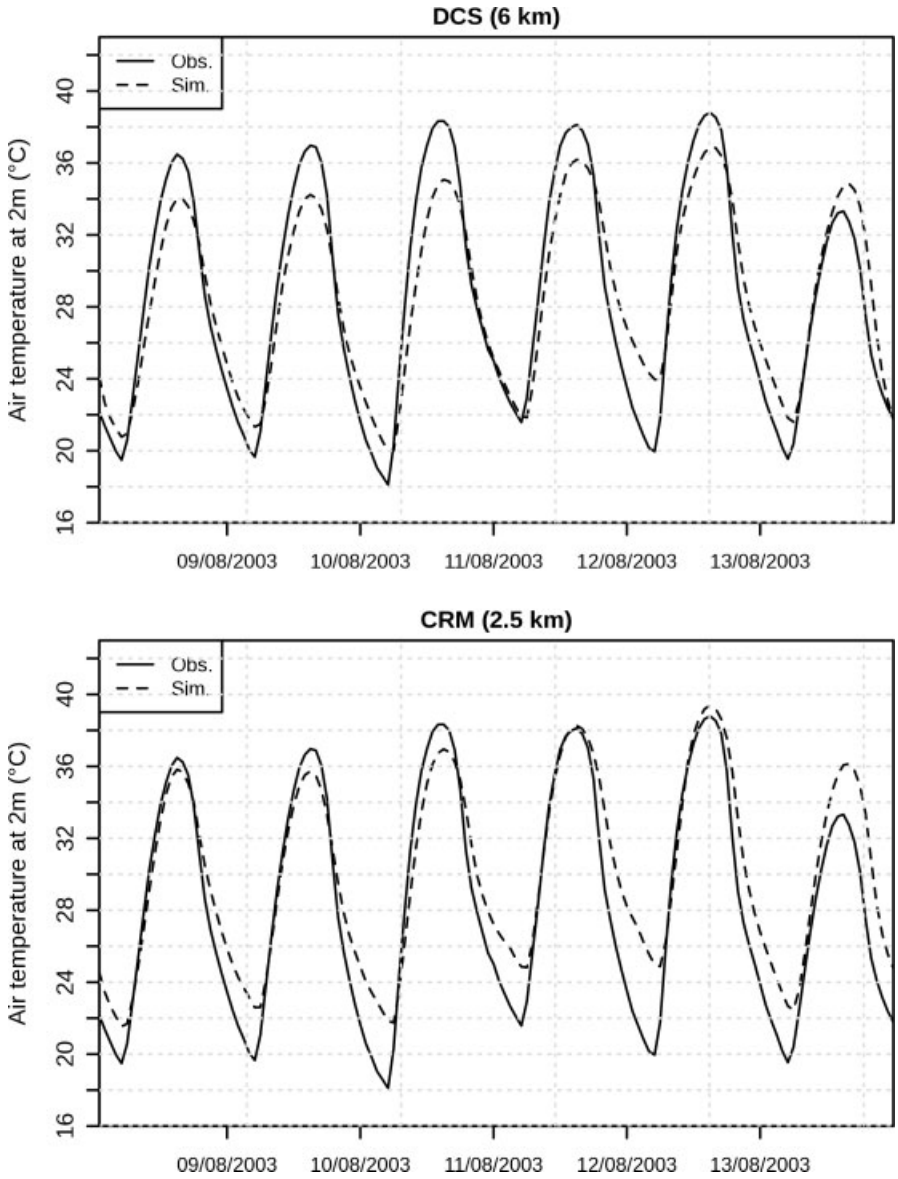

Figure A2. Mean (across 63 weather stations) 2-m air temperatures observed and simulated with a Deep Convection Scheme (DCS) configuration running at a 6 km spatial resolution (top) and with a Cloud Resolving Model (CRM) running at a 2.5 km spatial resolution (bottom), between the 8 and 14 of August 2003.

The two configurations were also compared in terms of simulating 2-m air temperatures, based on 63 weather stations located about the IDF domain. Although both configurations have a similar root mean square error (around 3 °C, Table AI), they do not present the same mean bias. The difference in mean bias between the two configurations (almost 0 °C for the DCS and 2.7 °C for the CRM) is illustrated in Figure A2, which presents mean time series of observed and simulated 2-m air temperatures (mean across the 63 stations). For the two configurations, the daily cycle of temperatures is well reproduced. In the case of the DCS configuration, the simulated temperatures show a tendency of this parameterisation to overestimate daily minima and underestimate daily maxima in similar proportions, resulting in an almost zero bias. The CRM configuration also overestimates the minima of temperatures, but in that case, this overestimation is not compensated by an underestimation of maxima which are better simulated. This results in a greater bias (1.5 °C) than for the DCS configuration, but this value is acceptable at this spatial resolution.

Table AI. Statistics on the agreement between simulated and observed 2-m air temperatures for the two FR model configurations tested and for an ensemble of 63 weather stations. RMSE stands for Root Mean Square Error, DSC for Deep Convection Scheme, CRM for Cloud Resolving Model.

Statistic	Model configuration	
	DCS (at 6 km)	CRM (at 2.5 km)
RMSE on T (°C)	2.7	3.0
Mean bias on T (°C)	−0.0	1.5

Given these results, the CRM configuration running at a 2.5 km resolution was chosen as being the most realistic regarding the simulation of sporadic storm events, and able to reproduce correctly air temperatures at 2 m, although differences remain between observed and simulated daily minima.

References

Adnot J. 2003a. *Energy Efficiency and Certification of Central Air Conditioners. Study for the D.G. Transportation-Energy (DGTREN) of the Commission of the EU*. Ed. ARMINES. Final report, vol 1, April 2003, 1–54.

Adnot J. 2003b. *Energy Efficiency and Certification of Central Air Conditioners. Study for the D.G. Transportation-Energy (DGTREN) of the Commission of the EU*. Ed. ARMINES. Final report, vol 3, April 2003, 1–91.

Akbari H, Konopacki S. 2004. Energy savings of heat-island reduction strategies in Toronto, Canada. *Energy* **29**: 191–210.

Akbari H, Pomerantz M, Taha H. 2001. Cool surfaces and shade trees to reduce energy use and improve air quality in urban areas. *Solar Energy* **70**(3): 295–310.

APUR (Atelier Parisien d'Urbanisme). 2007. *Consommation d'énergie et émissions de gaz à effet de serre liées au chauffage des résidences principales parisiennes*. Atelier Parisien d'Urbanisme: Paris, décembre 2007, 1–46.

Bessemoulin P, Bourdette N, Courtier P, Manach J. 2004. La canicule d'août 2003 en France et en Europe. *La Météorologie* **46**: 25–33.

Bougeault P, Lacarrère P. 1989. Parameterization of orography-induced turbulence in a meso-beta scale model. *Monsoon Weather Review* **117**: 1872–1890.

Charnock H. 1955. Wind stress on a water surface. *Quarterly Journal of the Royal Meteorological Society* **81**: 639–640.

Colombert M. 2008. *Contribution à l'analyse de la prise en compte du climat urbain dans les différents moyens d'intervention sur la ville*. Thèse de l'Université Paris-Est.

Cuxart J, Bougeault Ph, Redelsperger JL. 2000. A turbulence scheme allowing for mesoscale and large-eddy simulations. *Quarterly Journal of the Royal Meteorological Society* **126**: 1–30.

Dousset B, Gourmelon F, Laaidi K, Zeghnoun A, Giraudet E, Bretin P, Mauri E, Vandentorren S. 2011. Satellite monitoring of summer heat waves in the Paris metropolitan area. *International Journal of Climatology* **31**(2): 313–323.

Efron B, Tibshirani R. 1993. *An Introduction to the Bootstrap*. Chapman and Hall: New York, London.

Habets F, Boone A, Champeaux JL, Etchevers P, Franchistéguy L, Leblois E, Ledoux E, Le Moigne P, Martin E, Morel S, Noilhan J, Quintana Segui P, Rousset-Regimbeau F, Viennot P. 2008. The SAFRAN-ISBA-MODCOU hydrometeorological model applied over France. *Journal of Geophysical Research* **113**: DOI: 10.1029/2007JD008548.

Hamdi R, Masson V. 2008. Inclusion of a Drag Approach in the Town Energy Balance (TEB) Scheme: Offline 1D Evaluation in a Street Canyon. *Journal of Applied Meteorology and Climatology* **47**: 2627–2644.

Hassid S, Santamouris M, Papanikolaou N, Linardi A, Klitsikas N, Georgakis C, Assimakopoulos DN. 2000. The effect of the Athens heat island on air conditioning load. *Energy and Buildings* **32**: 131–141.

Hohenegger C, Schär C. 2007. Predictability and error growth dynamics in cloud-resolving models. *Journal of Atmospheric Science* **64**: 4467–4478.

Hsieh C-M, Aramaki T, Hanaki K. 2007. The feedback of heat rejection to air conditioning load during the nighttime in subtropical climate. *Energy and Building* **39**: 1175–1182.

Kain JS, Fritsch JM. 1993. Convective parameterization for mesoscale models: The Kain-Fritsch scheme. *Meteorological Monographs* **46**: 165–170.

Kikegawa Y, Genchi Y, Yoshikado H, Kondo H. 2003. Development of a numerical simulation system toward comprehensive assessments of urban warming countermeasures including their impacts upon the urban buildings' energy-demands. *Applied Energy* **76**: 449–466.

Kolokotroni M, Giannitsaris I, Watkins R. 2006. The effect of the London urban heat island on building summer cooling demand and night ventilation strategies. *Solar Energy* **80**: 383–392.

Lafore JP, Stein J, Asencio N, Bougeault P, Ducrocq V, Duron J, Fischer C, Héreil P, Mascart P, Masson V, Pinty JP, Redelsperger JL, Richard E, de Arellano JV-G. 1998. The Méso-NH atmospheric simulation system. Part I: adiabatic formulation and control simulation. *Annales Geophysicae* **16**: 90–109.

Ledrans M, Vandentorren S, Bretin P, Croisier A. 2005. Etude des facteurs de risque de décès des personnes âgées résidant à domicile durant la vague de chaleur d'août 2003. Rapport de l'Institut national de Veille Sanitaire. pp 1–116. ISBN: 2-11-094963-5.

Lemonsu A, Bélair S, Mailhot J, Leroyer S. 2010. Evaluation of the Town Energy Balance Model in Cold and Snowy Conditions during the Montreal Urban Snow Experiment 2005. *Journal of Applied Meteorology and Climatology* **49**: 346–362.

Lemonsu A, Grimmond CSB, Masson V. 2004. Modeling the surface energy balance of the core of an old Mediterranean city: Marseille. *Journal of Applied Meteorology* **43**: 312–327.

Masson V. 2000. A physically-based scheme for the urban energy budget in atmospheric models. *Boundary-Layer Meteorology* **94**: 357–397.

Masson V, Champeaux JL, Chauvin F, Meriguet C, Pigeon G. 2003. ECOCLIMAP: a global database of land surface parameters at 1-km resolution in meteorological and climate models. *Journal of climate* **16**(9): 1261–1282.

Masson V, Grimmond CSB, Oke TR. 2002. Evaluation of the Town Energy Balance (TEB) scheme with direct measurements from dry districts in two cities. *Journal of Applied Meteorology* **41**: 1011–1026.

Masson V, Seity Y. 2009. Including atmospheric layers in vegetation and urban offline surface schemes. *Journal of Applied Meteorology and Climatology* **48**: 1377–1397.

Noilhan J, Mahfouf JF. 1996. The ISBA land surface parameterisation scheme. *Global and Planetary Change* **13**: 145–159.

Offerle B, Grimmond CSB, Fortuniak K. 2005. Heat storage and anthropogenic heat flux in relation to the energy balance of a central European city centre. *International Journal of Climatology* **25**: 1405–1419.

Ohashi Y, Genshi Y, Kondo H, Kikegawa Y, Yoshikado H, Hirano Y. 2007. Influence of air-conditioning waste heat on air temperature in Tokyo during summer: numerical experiments using an urban canopy model coupled with a building energy model. *Journal of Applied Meteorology and Climatology* **46**: 66–81.

Pergaud J, Masson V, Malardel S, Couvreux F. 2009. A parameterization of dry thermals and shallow cumuli for mesoscale numerical weather prediction. *Boundary-Layer Meteorology* **132**: 83–106.

Pigeon G, Legain D, Durand P, Masson V. 2007. Anthropogenic heat releases in an old European agglomeration (Toulouse, France). *International Journal of Climatology* **27**: 1969–1981.

Pigeon G, Moscicki MA, Voogt JA, Masson V. 2008. Simulation of fall and winter surface energy balance over a dense urban area using the TEB scheme. *Meteorology and Atmospheric Physics* **102**: 159–172.

R Development Core Team. 2010. *R: A language and environment for statistical computing. R Foundation for Statistical Computing*. Vienna, Austria. ISBN: 3-900051-07-0. URL: http://www.R-project.org.

Salamanca F, Martilli A, Tewari M, Chen F. 2011. A Study of the urban boundary layer using different urban parameterizations and high-resolution urban canopy parameters with WRF. *Journal of Applied Meteorology and Climatology* **50**: 1107–1128, DOI: 10.1175/2010JAMC2538.1.

Stein J, Richard E, Lafore J, Pinty J, Asencio N, Cosma S. 2000. High -resolution non-hydrostatic simulations of flash-flood episodes with grid-nesting and ice-phase parametrization. *Meteorolology and Atmospheric Physics* **72**: 101–110.

Sullivan PP, Moeng C-H, Stevens B, Lenschow DH, Mayor SD. 1998. Structure of the entrainment zone capping the convective atmospheric boundary layer. *Journal of the Atmospheric Sciences* **55**: 3042–3064.

Wen Y, Lian Z. 2009. Influence of air conditioners utilization on urban thermal environment. *Applied Thermal Engineering* **29**: 670–675.

